The Structure and Porosity of $Fe_{62-x}Co_{10}W_yMe_xY_8B_{20-y}$ Alloys in the Amorphous and Crystalline States (where: Me = Mo, Nb; x = 0, 1, 2; y = 0, 1, 2)

MARCIN NABIALEK[1], PAWEL PIETRUSIEWICZ[1]*, MICHAL SZOTA[2], MOHD MUSTAFA AL BAKRI ABDULLAH[3,4], ANDREI VICTOR SANDU[3,4]*

[1] Institute of Physics, Faculty of Production Engineering and Materials Technology, Czestochowa University of Technology, 19 Armii Krajowej Str., 42-200 Czestochowa, Poland

[2]Institute of Materials Science and Engineering. Department of Materials Processing Technology and Applied Physics, Czêstochowa University of Technology, 19 Armii Krajowej Str., 42-200 Czêstochowa

[3] Geopolymer & Green Technology (CeGeoGTech), School of Material Engineering, Universiti Malaysia Perlis (UniMAP), 01000 Kangar, Perlis Malaysia

[4] Gheorghe Asachi Technical University of Iasi, Faculty of Materials Science and Engineering, 41 D. Mangeron Blvd., 70050, Iasi, Romania

The investigated crystalline and amorphous samples were obtained by crystallization of the liquid alloy on a water-cooled copper plate and by an injection-casting method, respectively. In each case, the structure of the samples was determined by examination of the obtained X-ray diffraction patterns. The diffraction patterns of samples produced by the injection casting method were characterized by a single broad peak called the amorphous halo. The samples produced by the crystallization method were shown to feature within their structure the following phases: YB_2, Fe_2Y, á-Fe, Co_5Y, and B_6Co_{23}. Further research, performed using computer tomography, revealed the existence of pores within the samples. The crystalline-structure samples were found to feature a lower average pore diameter.

Keywords: Amorphous materials, metals and alloys, Bulk metallic glasses, Computed tomography, microstructure, X-ray diffraction

For over 50 years, intensive research has been undertaken with the aim of characterising amorphous structure and, further, nanocrystalline structure, the latter consisting of mixtures of both amorphous and crystalline' phases [1-3]. It is well known that, for a nanocrystalline material, the best properties are observed if there is homogeneous distribution of the crystalline grains within an amorphous matrix [4, 5]. This is based on the assumption that the size of these grains is less than 100 nm in one of the determined directions [4, 6, 7]. The manufacturing process of amorphous and nanocrystalline materials is complicated and requires specialist equipment [5, 7-11].

For more than a decade, research has been carried out at the Czestochowa University of Technology with the aim of establishing the parameters of a single-step production process for creating nanocrystalline materials [12]. Defects, created during the production process of the materials, have also been investigated. It has been found that the solidification time of the molten alloy is a very important parameter, influencing not only the creation of the amorphous state, but also the size of the resulting pores in the structure.

In this work, the results are presented of X-ray and computer tomography investigations, performed on rapidly-quenched alloys that exhibit soft magnetic properties [13, 14]. Due to their potential applications in the electrical and electronic industries (for example, in transformer cores or as elements of micro-devices) these alloys feature as an extensively-researched group of materials [15, 16]. These materials are usually obtained in the form of thin ribbons, through the application of a melt-spinning method [17, 18]. Unfortunately, the obtained ribbon constitutes an open-circuit sample, and in order to close the magnetic circuit, it has to be coiled. In addition, ribbons are produced at quenching speeds of 10^4-10^5 K/s. The "freezing" of the structure within the amorphous state causes the introduction of short- and medium-range stresses. The presence of these stresses results in some deterioration of the soft magnetic properties of the ferromagnetic material [19]. Improvement in the soft magnetic properties could be achieved by an additional thermal treatment, resulting in partial relaxation of the structure and the releasing of free volumes and quasidislocational dipoles to the surface of the sample [20-25]. The other way to achieve a relaxed structure could be the manufacturing process itself. Frequently, the quality and type of structure can be determined by directional cooling, leading to the columnar growth of crystals, for example in AlNiCo magnets. Unfortunately, for the majority of alloys, an amorphous structure or nanocrystalline structure with homogeneous grain distribution could not be produced. Reduction of the quenching speed (10^1-10^2 K/s) and improvement of the glass-forming abilities have been achieved using alternative production methods, such as the suction- or injection-casting of the alloy into a copper die. Utilisation of these methods, in conjunction with the right chemical composition of the alloy, can yield a resulting material featuring an amorphous or nanocrystalline structure with a partially-relaxed structure - without the need for additional thermal treatment [26-32]. In addition, a sample can be obtained with an inherently closed magnetic circuit.

The aim of this work was to investigate the defects within the structure of alloys made by respective

* email: pietrusiewicz@wip.pcz.pl; sav@tuiasi.ro

unidirectional and radial cooling of the liquid material; further, to determine the effect of the quenching speed on the thermodynamics of the nucleation of the crystalline grains and the resulting grain size.

Experimental part

The samples used in the investigations were made using high-purity component elements: Fe – 99.98 at %, Co – 99.98 at%, W- 99.9999 at %, Y- 99.98 at %, Mo – 99.9999 at %, Nb – 99.98 at %. The element boron was added as an alloy of known composition, i.e. $Fe_{45.4}B_{54.6}$. The liquid alloy was solidified using two respective methods: in the copper die using the injection-casting method (radial cooling) and on the copper plate (unidirectional cooling).

The structure of the obtained samples was investigated using an X-ray diffractometer (Bruker Advance D8) over the 2Θ range from 30 to100° and using a measurement step of 0.02° (CuK_α(λ = 1.54056Å)).

Analysis of the volume structural defects (in the form of pores) was carried out by computer microtomography, using a BrukerSkyScan1172. This experiment was performed using a voltage of 100 kV between the cathode and anode of the tungsten Roentgen lamp. The current had a value of 100 μA, the rotation step around the sample was 0.3° (from 0 to 360°) and the exposure time was 1.2s. The obtained resolution was 2.38 μm.

The single radiograph was an average produced from 6 projections. The samples that had been quenched in the copper die in the form of cuboids had dimensions of: 10 mm × 10 mm × 1 mm; from a central point on each of these investigated samples, a cuboid with dimensions of: 1.19mm×1.19mm×0.238 mm was analysed (fig. 1b). In the case of the samples cooled on the copper plate, a zone in the centre of each sample, 3 mm above the contact point with the copper plate, was analysed (fig. 1c).

The mean grain size D for the crystalline phases present in the volume of each sample was estimated using the Scherrer equation [33-35]:

$$D = \frac{\lambda K}{B_0 \cos\Theta}$$

where:

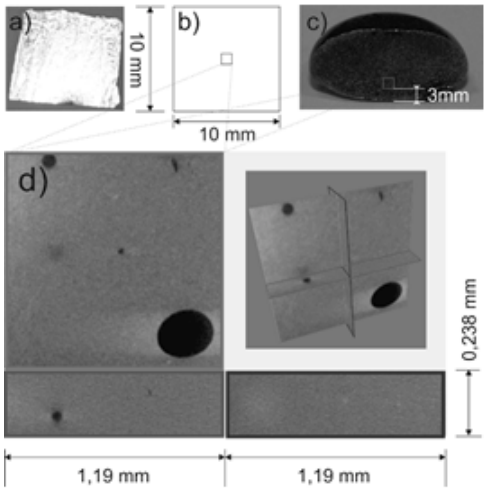

Fig. 1. Sample preparation for the computer tomography investigations: a) sample obtained by rapid quenching in the copper die, b) marked area used in the experiment, c) cross-section of the sample obtained by unidirectional cooling with area used in the experiment marked, d) example of a studied area

K –dimensionless shape factor (assumed K = 0.9);

λ –X-ray wavelength;

B_0 – line broadening at half the maximum intensity (including the background);

Θ – Bragg's angle.

Results and discussions

The computer tomography investigations were used to reveal the percentage contribution of pores within the selected area of each alloy sample; table 1 shows the results for the samples produced by rapid quenching of the liquid alloy on the copper plate, and table 2 shows those for the samples produced in the copper die. It was found that, within the volume of the injection-cast sample, there was a higher number of pores present, in comparison to the sample produced by cooling on the copper plate. This can be explained by the sample production process itself. In the injection-casting method, the liquid alloy is injected into the copper die using pressurised argon gas; the alloy is

Alloy composition	Cooling on the copper plate	
	Pore contribution [%]	Average pore diameter [μm]
$Fe_{62}Co_{10}Y_8B_{20}$	0.1	7.9
$Fe_{61}Co_{10}Mo_1Y_8B_{20}$	<0.01	4.77
$Fe_{60}Co_{10}Mo_2Y_8B_{20}$	0.03	10.35
$Fe_{60}Co_{10}W_1Mo_2Y_8B_{19}$	0.1	8.21
$Fe_{60}Co_{10}W_2Mo_2Y_8B_{18}$	<0.01	5.6
$Fe_{61}Co_{10}Nb_1Y_8B_{20}$	<0.01	4.77
$Fe_{60}Co_{10}Nb_2Y_8B_{20}$	<0.01	3.57
$Fe_{60}Co_{10}W_1Nb_2Y_8B_{19}$	0.31	72.28
$Fe_{60}Co_{10}W_2Nb_2Y_8B_{18}$	<0.01	6.5

Table 1
PERCENTAGE CONTRIBUTION OF PORES TO THE VOLUME OF EACH ALLOY AND VALUES OF THE AVERAGE PORE DIAMETER FOR THE ALLOYS PREPARED USING THE COPPER PLATE METHOD

Alloy composition	Cooling in the copper die	
	Pore contribution [%]	Average pore diameter [μm]
$Fe_{62}Co_{10}Y_8B_{20}$	<0.01	12.4
$Fe_{61}Co_{10}Mo_1Y_8B_{20}$	0.64	115.21
$Fe_{60}Co_{10}Mo_2Y_8B_{20}$	0.1	15.67
$Fe_{60}Co_{10}W_1Mo_2Y_8B_{19}$	0.17	42.39
$Fe_{60}Co_{10}W_2Mo_2Y_8B_{18}$	0.1	21.31
$Fe_{61}Co_{10}Nb_1Y_8B_{20}$	0.17	57.39
$Fe_{60}Co_{10}Nb_2Y_8B_{20}$	0.31	72.2
$Fe_{60}Co_{10}W_1Nb_2Y_8B_{19}$	2.7	188.8
$Fe_{60}Co_{10}W_2Nb_2Y_8B_{18}$	0.12	14.5

Table 2
PERCENTAGE CONTRIBUTION OF PORES TO THE VOLUME OF EACH ALLOY AND VALUES OF THE AVERAGE PORE DIAMETER FOR THE ALLOYS PREPARED BY COOLING IN THE COPPER DIE

then solidified at a rate of approximately 10^1–10^2 K/s. It is considered very likely that, during the injection process, argon is mixing with the liquid alloy, and becoming *trapped* during the solidification of the alloy.

For the majority of the investigated alloys, the percentage contribution of pores within the studied volume is over tenfold lower for the samples quenched on the copper plate. In addition, the average diameter of pores in the samples obtained by injection-casting is significantly higher for the samples cooled in the copper die. This suggests that the production technique of the ultrafast-cooled alloys is the major factor influencing creation of imperfections in the internal structure. It is important to mention that cooling within the copper die occurs radially, whereas on the copper plate it is unidirectional. In the case of the radial coolingprocess (at 10^1–10^2 K/s), the quenching dynamics are the same in all directions; this hinders relaxation of the structure occurring in the alloy volume. This applies to structural relaxation on the elementary level as well as relaxation of the larger imperfections, such as pores. A completely different description of relaxation processes applies to alloys that are cooled in one direction only; the sample is solidified starting from the cooling surface of the copper plate towards the top. As suggested by the results of the experiments, the majority of the pores are moving in the same direction, being released to the sample surface. The decrease in the quenching rate, towards the limit of the creation of the glass state, results in the nucleation of crystalline grains and their growth. This occurs in the investigated alloys. Figures 2 and 3 show X-ray diffraction patterns for the alloys produced by the injection-casting method.

In the case of the alloys with amorphous structure and with short-range interactions between the atoms, the X-ray diffraction patterns do not feature any narrow peaks that would indicate crystalline phases (fig. 2 and fig. 3). Instead, these patterns obtained for the amorphous alloys consist of a single, wide maximum: the so-called amorphous halo. The Röntgen rays are dispersed by the randomly distributed atoms in the amorphous materials

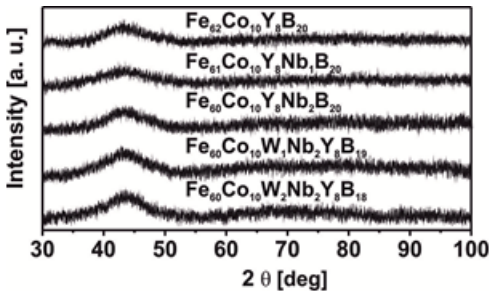

Fig.2. X-ray diffraction patterns for the samples obtained by injection-casting. The group featuring the addition of Nb is shown.

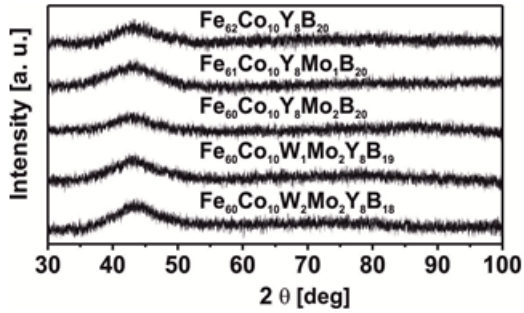

Fig. 3. X-ray diffraction patterns for the samples of alloys produced by cooling in the copper die. The group featuring the addition of Mo is shown

with no elementary cell. Therefore the recorded dispersion of the X-rays by the amorphous structure is wide, softening the maximum with a lower overall intensity [36, 37].

Figures 4 and 5 show X-ray diffraction patterns for the samples of both groups of the investigated alloys that were produced by cooling on the copper plate.

The X-ray diffraction patterns recorded for the samples quenched on the copper plate consist of a low-intensity background and clear, narrow peaks; this confirms the presence of crystalline structure (fig. 4 and 5).

In the case of the alloys produced on the cooled plate, a fine grain structure with grains of less than 100μm is expected. In general, for the investigated alloys quenched on the copper plate, which are polycrystalline, the principal

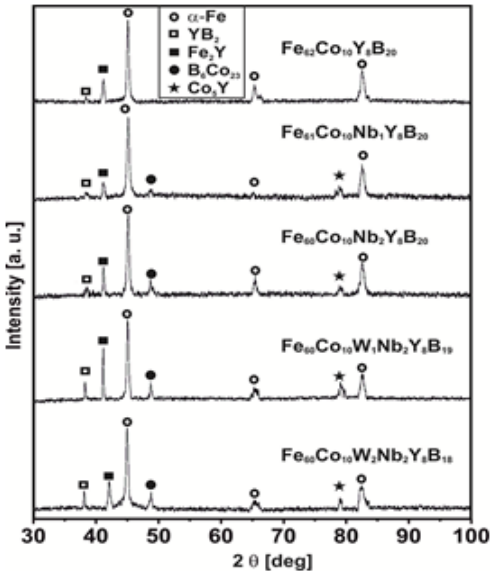

Fig. 4. X-ray diffraction patterns for the samples made by cooling on the copper plate. The group featuring the addition of Nb is shown

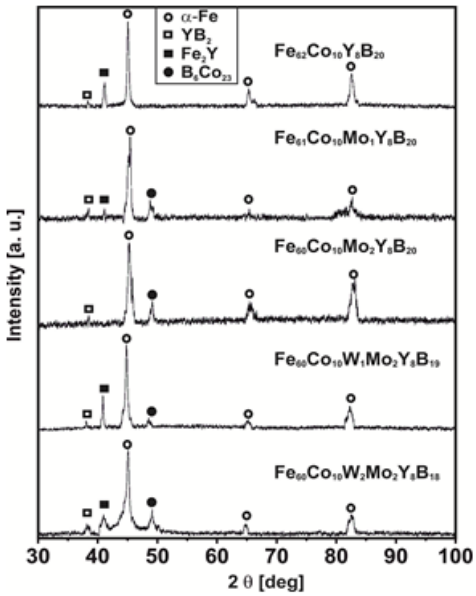

Fig. 5. X-ray diffraction patterns for the samples made by cooling on the copper plate. The group featuring the addition of Mo is shown

process of nucleation- homogeneous nucleation -can be assigned. During the relatively rapid solidification of the liquid alloy and due to fluctuations in the chemical composition, nucleation of the crystalline grains and creation of short-range order occur. The areas which feature fluctuations in the composition and density are very small and, with time, cluster structures are created. It is

Table 3

THE AVERAGE VALUES OF GRAIN SIZE, ESTIMATED USING THE SCHERRER EQUATION, FOR THE SAMPLES OF BOTH GROUPS OF ALLOYS THAT WERE COOLED ON THE COPPER PLATE

Alloy composition	Estimated average grain size D [nm]				
	YB_2	Fe_2Y	Fe	Co_5Y	B_6Co_{23}
$Fe_{62}Co_{10}Y_8B_{20}$	523	616	608	–	–
$Fe_{61}Co_{10}Mo_1Y_8B_{20}$	548	1018	372	–	273
$Fe_{60}Co_{10}Mo_2Y_8B_{20}$	591	–	356	–	525
$Fe_{60}Co_{10}W_1Mo_2Y_8B_{19}$	642	808	462	–	382
$Fe_{60}Co_{10}W_2Mo_2Y_8B_{18}$	441	355	608	–	366
$Fe_{61}Co_{10}Nb_1Y_8B_{20}$	374	411	489	1308	366
$Fe_{60}Co_{10}Nb_2Y_8B_{20}$	548	837	566	1207	366
$Fe_{60}Co_{10}W_1Nb_2Y_8B_{19}$	775	1018	656	957	557
$Fe_{60}Co_{10}W_2Nb_2Y_8B_{18}$	864	616	754	1075	557

Table 4

PERCENTAGE CONTRIBUTION OF THE CRYSTALLINE PHASES

Alloy composition	Percentage contribution (%)				
	YB_2	Fe_2Y	Fe	Co_5Y	B_6Co_{23}
$Fe_{62}Co_{10}Y_8B_{20}$	0.9	8.0	91.1	-	-
$Fe_{61}Co_{10}Mo_1Y_8B_{20}$	2.8	2.2	88.8	-	6.2
$Fe_{60}Co_{10}Mo_2Y_8B_{20}$	1.5	-	92.7	-	5.7
$Fe_{60}Co_{10}W_1Mo_2Y_8B_{19}$	1.1	13.3	84.2	-	1.5
$Fe_{60}Co_{10}W_2Mo_2Y_8B_{18}$	1.3	6.4	83.5	-	8.8
$Fe_{61}Co_{10}Nb_1Y_8B_{20}$	1.6	4.8	88.4	3.4	1.9
$Fe_{60}Co_{10}Nb_2Y_8B_{20}$	0.3	9.5	83.9	1.4	4.9
$Fe_{60}Co_{10}W_1Nb_2Y_8B_{19}$	3.9	23.7	64.7	4.0	3.7
$Fe_{60}Co_{10}W_2Nb_2Y_8B_{18}$	4.3	9.5	78.9	2.9	4.4

very interesting that, within these clusters, the atomic distribution is similar to that of the atom with the highest proportion in the given solidified fluctuation of the chemical composition. After delivery to the system of a quantity of energy facilitating the atomic diffusion, and therefore an increase in the distance of the interactions between them, the growth of the preferred crystallites within the system occurs. That is why several crystalline phases with different grain sizes could be observed within the investigated alloys.

Each of the sharp maxima on the X-ray diffraction patterns has been identified and assigned to a specific crystalline phase using the EVA software and the specialist database ICDD PDF-4+ Release 2013. The dominant crystalline phase in the investigated alloys is the α-Fe crystalline phase. This means that the standard crystallisation process of the alloy type FeCoB has been preserved [38-43]. These alloys crystallise in two stages: i.e.: primary and secondary crystallisation. During primary crystallisation, precipitation of the α-Fe crystalline phase grains occurs; with time, these grains reach dimensions of a few hundred nanometres. During the further growth of the α-Fe crystalline grains, the extended cooling time allows crystalline grains of different phases featuring the element Y to be created within the volume of the sample, i.e. YB_2, Fe_2Y, Co_5Y**.** These three phases are created during the secondary crystallisation. Another effect of the rapid cooling on the copper plate is the presence, in minute quantities, of the trigonal, embryonic metastable B_6Co_{23} phase, the nuclei of which were *frozen* during the solidification process.

The presence of metastable phases in the investigated alloys suggests that the crystallization process has not been completed.

The values of grain size of the individual phases within samples of the alloys which were cooled on the copper plate were estimated using the Scherrer equation and are gathered in table 3.

It should be noted that the estimated average crystalline grain size for the phases Fe and B_6Co_{23} are smaller for the alloys without the addition of tungsten. Addition of between 1 and 2 at. % of tungsten enhances the crystallisation process of the aforementioned crystalline phases and causes rapid growth of the crystalline grains of these phases.

The dominant crystalline phase in both groups of the investigated alloys is the α-Fe crystalline phase with the % contribution being several times higher than all the remaining phases (table 4). As has already been mentioned, the crystalline phase remaining after the production process is metastable B_6Co_{23}, for which the % contribution in the first group of alloys is less than 9%. Introduction to the base alloy of between 1 and 2 at. % of the alloying elements improves the likelihood of the creation of the crystalline phases. In the first group of the alloys, this results in the creation of one additional crystalline phase, namely B_6Co_{23}; in the second group of the alloys, in addition to the B_6Co_{23} crystalline phase, the Co_5Y crystalline phase has also been created. In general, the element Mo is added to the alloys to hinder growth of the crystalline grains, particularly dendrites, and it is causing structural refinement [44].

The described effect has been achieved for the crystalline phase with the major contribution in these alloys - α-Fe. In the base alloy, the average size of the crystalline grains of the á-Fe crystalline phase has almost halved: $Fe_{62}Co_{10}Y_8B_{20}$ –608nm→$Fe_{61}Co_{10}Mo_1Y_8B_{20}$ – 372nm→ $Fe_{60}Co_{10}Mo_2Y_8B_{20}$ – 356nm. In addition, the percentage contribution ofthe á-Fe crystalline phase has increased by a few percent. It could be stated that an addition of 2 at. % of Mo to the base alloy is stabilizing the alloy structure during the solidification process and hindering the atomic diffusion. As an additional effect, in the $Fe_{60}Co_{10}Mo_2Y_8B_{20}$ alloy the crystalline phase Fe_2Y, present in the $Fe_{61}Co_{10}Mo_1Y_8B_{20}$ alloy, is eliminated. In addition,partial

decomposition of the metastable phase B_6Co_{23} and the YB_2 phase are found to occur.

After addition of 1 at. % of W to the alloy containing 2 at. % of Mo, the Fe_2Y phase reappears. Addition of 2 at. % of W resulted in refinement of the structure of the crystalline phases of: YB_2 , Fe_2Y and B_6Co_{23} when compared with the alloy containing 1 at. % of W.

In the second group of the alloys, in order to hinder growth of the crystalline grains, the element Nb was used. During the initial stages of crystallisation, Nb diffuses from the crystallisation front to the matrix between the crystalline grains [45, 46].

According to the results presented in table 3, the introduction of Nb to the base alloy has a different effect on the evolution of the crystalline phases when compared to the alloys with Mo.

Prevention of long-distance atomic diffusion resulted in the creation of the Co_2Y crystalline phase, which has not been observed in the first group. Moreover, it should be mentioned that, in comparison with the alloys containing Mo, for the alloys with added Nb the following changes have been observed: an increase in the average crystalline grain size for all identified phases, and decreases in the percentage contribution of:Y_2b, Fe_2Y and α-Fe phases. After the addition of W to the alloys containing Nb, a similar effect on the structural stability to that of the group of alloyswith Mo and added W has been observed.

Conclusions

In this work, samples of the alloys of $Fe_{62-x}Co_{10}W_yMe_xY_8B_{20-y}$ (where: Me = Mo, Nb; x = 0, 1, 2; y = 0, 1, 2), produced by two different production methods, have been investigated. The manufacturing processes differed in the mechanism of cooling the samples and the associated quenching speed. It has been shown that an extended quenching time allows the production of a sample with less pores and smaller pore dimensions. Unfortunately, the extended solidification time is also a reason for the crystallisation of samples.

Even given the addition of the alloying elements Mo and Nb, which are known for improving the glass-forming ability of alloys, an amorphous structure has not been achieved in the case of the alloys produced on the copper plate. Despite the fact that, using the described manufacturing techniques, the production of amorphous alloys wasn't the aim of the work, the authors were expecting to create a mixed structure with an amorphous matrix and crystallites no larger than a few tens of nanometres.

Based on the presented results of the investigations, it has been found that an increase in the packing density within the sample volume is an important parameter, influencing the properties of the alloy. The internal voids have a negative impact on the durability parameters of samples and are the cause of crack-propagation. In the case of magnetic materials, voids increase hysteresis losses and cause uneven flow of the magnetic field within the sample volume– which, in turn, can result in overheating of the material.

The aforementioned conclusions explain why it is important to develop production methods which facilitate reductions in the quantity and size of pores within the produced material. This is especially important for magnetic materials, where the produced object has a volume and is closed in the magnetic context.

Acknowledgment: The authors would like to thank Dr. eng. Sebastian Garus for the part of the material reaserch results.

References

1.MORENO RAMIUREZ, L.M., BLAZQUEZ, J.S., FRANCO, V., CONDE, A., MARSILIUS, M., BUDINSKY, V., HERZER, G., Journal of Magnetism and Magnetic Materials, 409, 2016, p. 56.
2.YOSHIZAWA, Y., OGUMA, S., YAMAUCHI, K., J. Appl. Phys. 64, 1988, p. 6044.
3.KULIK, T., VLASAK, G., ZUBEREK, R., Materials Science and Engineering A, 226-228, 1997, p. 701.
4.KULIK, T., HERNANDO, A., Journal of Magnetism and Magnetic Materials, 138, 1994, p. 270.
5.GHEIRATMAND, T., MADAAH HOSSEINI, H.R., Journal of Magnetism and Magnetic Materials, 408, 2016, p. 177.
6.POZO LOPEZ, G., FABIETTI, L.M., CONDO, A.M., URRETA, S.E., Journal of Magnetism and Magnetic Materials, 322, 2010, p. 3088.
7.KULIK, T., Journal of Non Crystalline Solids, 287, 2001, p. 145.
8.WANG, A., ZHAO, C., MEN, H., HE, A., CHANG, C., WANG, X., LI, R.W., Journal of Alloys and Compounds, 630, 2015, p. 209.
9.RÍOS, C.T., DE SOUZA, J. S., ANTUNES, R.A., Journal of Alloys and Compounds, 682, 2016, p. 412.
10.CHENG, C.Y., YEH, J.W., Materials Letters, 181, 2016, p. 223.
11.LU, Z.P., LIU, C.T., Journal of Materials Science, 39, 2004, p. 3965.
12.NABIALEK, M., PIETRUSIEWICZ, P., BLOCH, K., Journal of Alloys and Compounds, 628, 2015, p. 424.
13. HAN, Y., DING, J., KONG, F.L., INOUE, A., ZHU, S.L., WANG, Z., SHALAAN, E., AL-MARZOUKI, F., Journal of Alloys and Compounds, 691, 2017, p. 364.
14. LI, L.J., WANG, Z., HAN, Y., Materials Letters, 185, 2016, p. 235.
15.MCHENRY, M.E., WILLARD, M.A., LAUGHLIN, D.E., Progress in Materials Science, 44, 1999, p. 291.
16.DRABOLD, D.A., The European Physical Journal B, 68, 2009, p. 1
17.MINIC, D.M., MARICIC, A., Materials Science and Engineering B, 172, 2010, p. 127.
18.NABIALEK, M.G., PIETRUSIEWICZ, P., DOSPIA£, M.J., SZOTA, M., B£OCH, K., GRUSZKA, K., O•GA, K., GARUS, S., Journal of Alloys and Compounds, 615, 2014, p. S51
19. HUG, E., HUBERT, O., J.J. VAN HOUTTE, Materials Science and Engineering A, 332, 2002, p. 193.
20. KRONMÜLLER, H., FAHNLE, M., Micromagnetism and the microstructure of ferromagnetic solids, Cambridge University Press 2003.
21.KRONMÜLLER, H., J. Appl. Phys., 52, 1981, p. 1859.
22. TOKLOSA, Z., KWAPULINSKI, P., RASEK, J., HANECZOK, G., KUBISZTAL, M., Materials Science and Engineering B, 196, 2015, p. 1.
23.STOKLOSAA, Z., RASEK, J., KWAPULINSKI, P., BADURA, G., HANECZOK, G., PAJAK, L., LELATKO, J., KOLANO BURIAN, A., Journal of Alloys and Compounds, 509, 2011, p. 9050.
24. KWAPULINSKI, P., CHROBAK, A., HANECZOK, G., STOKLOSA, Z., RASEK, J., LELATKO, J., Materials Science and Engineering C, 23, 2003, p. 71.
25.CHEN, S. F., HUNG, C.Y., WANG, S.J., CHEN, S.H., CHEN, C.C., Journal of Alloys and Compounds, 627, 2015, p. 333.
26.BLOCH, K., J. Magn. Magn. Mater., 390, 2015, p. 118
27.BLOCH, K., NABIALEK, M., PIETRUSIEWICZ, P., GONDRO, J., DOŒPIAŁ, M., SZOTA, M., GRUSZKA, K., Acta Phys. Pol. A, 126, 2014, p. 108
28.INOUE, A., ZHANG, T., Mater. Trans. Jpn. Inst. Met., 36, 1995, p. 1184
29. TAKESHI, E., BILLINGE, S.J.L., Chapter 12 – Structure of Amorphous Materials, Pergamon Mater. Ser. 16 (2012) 455–465.
30. GARUS, S., NABIALEK, M., GARUS, J., Acta Phys. Pol. A, 126, 2014, p. 960
31.GARUS, S., NABIALEK, M., BLOCH, K., GARUS, J., Acta Phys. Pol. A, 126, 2014, p. 957.
32.GARUS, J., GARUS, S., NABIALEK, M., SZOTA, M., Acta Phys. Pol. A, 126, 2014, p. 954.
33.PATTERSON, A., Physical Review, 56, 1939, p. 978.
34.MOTE, V.D., PURUSHOTHAM, Y., Dole, B.N., J. Theor. Appl. Phys. 6, 2012, p. 1.

35. YASHPAL, S., SHARMA, V., MANOJ KUMAR, B.V., Materials Today: Proceedings, 2, 2015, p. 3534.
36. GRUSZKA, K., NABIALEK, M., BLOCH, K., OLSZEWSKI, J., Nukleonika, 60, 2015, p. 23.
37. BLOCH, K., NABIALEK, M., Acta Phys. Polon. A, 127, 2015, p. 442.
38. RAGHAVAN, V., Journal of Phase Equilibria and Diffusion, 33, 2012, p. 392.
39. ZHANG, J.T., WANG, W.M., LI, G.H., MA, H.J., QIN, J.Y., BIAN, X.F., Transactions of Nonferrous Metals Society of China, 20, 2010, p. 71.
40. AMIYA, K., URATA, A., NISHIYAMA, N., INOUE, A., Materials Science and Engineering A, 449–451, 2007, p. 356.
41. WANG, W.M., GEBERT, A., ROTH, S., KUEHN, U., SCHULTZ, L., Journal of Alloys and Compounds, 459, 2008, p. 203.
42. TAN, X.H., XU, H., BAI, Q., ZHAO, W.J., DONG, Y.D., Journal of Non-Crystalline Solids, 353, 2007, p. 410.
43. MAKINO, A., INOUE, A., MASUMOTO, T., Nanostructured Materials, 12, 1999, p. 825.
44. SHOROWORDI, K.M., BEPARI, M.M.A., Journal of Materials Engineering and Performance, 11, 2002, p. 625.
45. LI, X., LIU, J., QU, C., SONG, K., WANG, L., Journal of Alloys and Compounds, 694, 2017, p. 643.
46. XIANG, Z., WANG, A., ZHAO, C., MEN, H., WANG, X., CHANG, C., PAN, D., Journal of Alloys and Compounds, 622, 2015, p. 1000.

Manuscript received: 14.09.2016